Elucidating the weakly reversible Cs-Pb-Br perovskite nanocrystal reaction network with high-throughput maps and transformations

Authors: Jakob C. Dahl[1,3,4], Xingzhi Wang[1,3], Xiao Huang[1], Emory M. Chan[4], A. Paul Alivisatos[1,2,3,5,*]

1: Department of Chemistry and 2: Department of Materials Science and Engineering, University of California, Berkeley, California 94720, United States

3: Materials Sciences Division and 4: Molecular Foundry, Ernest Orlando Lawrence Berkeley National Laboratory, Berkeley, California 94720, United States

5: Kavli Energy NanoScience Institute, Berkeley, California 94720, United States

Abstract:

Advances in automation and data analytics can aid exploration of the complex chemistry of nanoparticles. Lead halide perovskite colloidal nanocrystals provide an interesting proving ground: there are reports of many different phases and transformations, which has made it hard to form a coherent conceptual framework for their controlled formation through traditional methods. In this work, we systematically explore the portion of Cs-Pb-Br synthesis space in which many optically distinguishable species are formed using high-throughput robotic synthesis to understand their formation reactions. We deploy an automated method that allows us to determine the relative amount of absorbance that can be attributed to each species in order to create maps of the synthetic space. These in turn facilitate improved understanding of the interplay between kinetic and thermodynamic factors that underlie which combination of species are likely to be prevalent under a given set of conditions. Based on these maps, we test potential transformation routes between perovskite nanocrystals of different shapes and phases. We find that shape is determined kinetically, but many reactions between different phases show equilibrium behavior. We demonstrate a dynamic equilibrium between complexes, monolayers and nanocrystals of lead bromide, with substantial impact on the reaction outcomes. This allows us to construct a chemical reaction network that qualitatively explains our results as well as previous reports and can serve as a guide for those seeking to prepare a particular composition and shape.

Introduction:

Data science and high-throughput experimentation have enabled rapid exploration in different areas of chemistry such as chemical biology,[1] drug discovery,[2] reaction discovery,[3] reaction optimization[4] and materials discovery.[5,6] Nanocrystal syntheses have additional complexity by adding different dimensionalities[7] to the multicomponent phase diagrams explored in more traditional bulk materials design.[8] Due to this complication, nanocrystal synthesis science has been mostly restricted to single-[7,9] or

two-component systems.[10–13] Lead halide perovskites[14–16] are three component systems and have a more complex and rich phase diagram, with nanocrystals of multiple species forming easily,[17,18] and chemical transformations between them accessible at or just above room temperature.[19–21] This makes them an ideal system to test whether we can increase our understanding of chemistry in complex nanocrystal phase diagrams by using automated synthesis and analysis methods.

The synthesis of lead halide perovskites can be controlled through a variety of parameters. Generally, such nanocrystals are made by addition of lead, cesium and bromide precursors to an alkane solution containing amine and carboxylate terminated alkyl moieties that act as agents to complex free metal ions or bind to the surfaces of any nanocrystallites.[22] Temperature and relative concentration of each of these species yields a synthetic space of large dimensionality. Prior studies established many interesting features of this space. Temperature can be used to tune the size of $CsPbBr_3$ nanocubes[22] and the thickness of $CsPbBr_3$ nanoplatelets.[23] While amine-free synthesis have been reported,[24] in the vast majority of synthesis in which amines are present they strongly influence the outcome. Amine chain length,[25] concentration[26] and protonation[26] are reported to control the formation of plates vis-a-vis cubes, their thickness as well as formation of the Cs_4PbBr_6 phase.[26] Secondary amines restrict the reaction entirely towards cubes.[27] Using ligand-assisted reprecipitation, cubes, plates, rods and spheres can all be made with variations in the chain length of the surfactant carboxylic acids and amines.[28] Further analysis suggested that it is ratios of lead to amine[29,30] and Cs to ammonium[26,31] that control the system rather than an absolute concentration of amine. In this work, we further explore how these and other factors interact with each other and build chemical understanding about why they matter.

The chemical transformations in this nanocrystal system are additional essential features of this system not usually observed for nanocrystals. Of particular importance is the reversible nature observed in the transformation between $CsPbBr_3$ and Cs_4PbBr_6.[20] The transformation from $CsPbBr_3$ to Cs_4PbBr_6 is accomplished through addition of oleylamine[19] and can be strongly accelerated by adding thiols[19] or thiocyanate,[32] switching from a process that takes seconds in an isotropic regime to taking hours or days in a more gentle layer-by-layer fashion depending on the chemical strength of the etchant solution. [32] The reverse transformation from Cs_4PbBr_6 to $CsPbBr_3$ can be induced by adding oleic acid or heat[20], solubilized $PbBr_2$,[17] or removing CsBr.[33] Additionally, a Br-deficient environment appears to lead to the formation of $CsPbBr_3$ through CsBr and Cs_4PbBr_6 intermediates,[34] suggesting that bromine might also induce transformation from Cs_4PbBr_6 to $CsPbBr_3$. Other transformations have also been observed: In a polar/nonpolar solvent mixture, $CsPbBr_3$ was shown to slowly transform to $CsPb_2Br_5$ after addition of dimethyldodecylammonium bromide.[21] These transformations are not confined to the Cs-Pb-Br phase

space. In the $CH_3NH_3PbX_3$ system, lead halide nanocrystals can be transformed into the perovskite material,[35,36] likely through intercalation reactions that are similar to those found in bulk.[37] Reversible transformation to metal-depleted species with amines was also observed with lead-free double perovskites nanocrystals.[38] We expand on these transformations and use them as qualitative measures to test which reactions are allowed, reversible or prohibited.

Integrating these diverse results into a cohesive picture has been difficult. Experimental work attempting to map out and integrate the synthesis has been limited, usually dealing with individual slices through the multidimensional synthesis landscape, such as the transition from synthesizing Cs_4PbBr_6 to $CsPbBr_3$,[30] or the formation of platelets of different sizes and cubes.[29] The first succeeded in directly mapping a small portion of a synthesis phase diagram, with the second using a machine learning model to give an approximation. The number of syntheses performed inherently limits the reliability and density of the maps produced – automated synthesis and analysis protocols can help gain better information. Previous studies display a single outcome dimension such as the ratio of Cs_4PbBr_6 to $CsPbBr_3$,[30] or average layer thickness of nanoplates,[29] or size of nanocubes,[26] which is useful to isolate a particular effect. Finding a way to display and reason with the multidimensional nature of this system is crucial to developing further and more coherent understanding.

This work explores the rich phase space of cesium lead bromide nanocrystal synthesis through factorial sets of 2337 synthesis experiments performed on a synthesis robot. An automated algorithm provides a deconvolution of absorption spectra into nine optically distinct species, from which we construct a detailed, multidimensional map of the synthetic space. We then traverse synthetic space: we test 149 transformations of the observed species upon addition of additional reagents. We observe an equilibrium of nanocrystalline, atomic layer and molecular lead halide phases which can serve as intermediates for the formation of different ternary cesium lead halide phases and geometries. This aids us in constructing a chemical reaction network that connects the synthesis and transformation reactions, explains the observation of multiple synthetic pathways, weakly reversible behavior and apparent non-linearity close to transition points. Finally, we discuss a range of observations from previous reports and find that our model has strong qualitative explanatory power, including over properties not initially considered. Our combination of high-throughput experimentation and quantitative analysis allows us to gain an overview of the reaction space, qualitatively analyze the transformations within this space, and build a more complete chemical understanding in the form of a chemical reaction network not apparent through either method alone.

Experimental:

Materials. Cesium acetate (99%), hexane (mixed isomers, 98+%) and ethyl acetate (≥99.5 %) were purchased from Fisher Scientific. Lead(II) acetate trihydrate (≥99.5%), benzoyl bromide (97%), oleic acid (technical grade, 90%), oleylamine (technical grade, 70%) and dodecane (99%) were purchased from Sigma-Aldrich. All chemicals were obtained from commercial suppliers and used without further purification.

Synthesis. Solutions of cesium (I) oleate (Cs-OA) and lead (II) oleate (Pb-OA) were prepared similar to a previous report.[39] Synthesis was performed through a modified version of the synthesis reported by Imran et al..[40] Briefly, solutions of lead oleate, cesium oleate, oleylamine and oleic acid were mixed in a 4 mL glass vial in hexanes. A stir bar was added, then the solution was stirred at room temperature and a benzoyl bromide solution was added to induce formation of nanocrystals. Nanocrystals were precipitated and resuspended in hexanes before further analysis. Further details in SI section 1.

Absorbance. UV-Vis absorption spectra of the cesium lead bromide species were recorded using a Shimadzu UV-3600 double beam spectrometer. Samples were prepared by diluting stock solutions of samples by a factor of 50 in hexanes. For each measurement, a blank spectrum was subtracted from the signal as background.

Powder X-ray diffraction (XRD) patterns of NCs were acquired using a Bruker D2 Phaser X-ray diffractometer equipped with a Cu Kα of 1.5445 A wavelength. Samples were prepared by drop-casting 100 ul stock solutions of NCs onto a silicon substrate. Samples were dried under air flow prior to measurements.

Transmission electron microscopy (TEM) images of the cesium lead bromide species were acquired using a FEI Tecnai T20 transmission electron microscope equipped with a Gatan RIO16IS camera and a LaB6 filament. All images were recorded under 200 kV accelerating voltage. Samples were prepared by dropcasting about 10 µL 1000 x diluted stock solutions onto a carbon support with 400 copper mesh. Samples were dried under ambient conditions prior to imaging.

High-throughput synthesis. For high-throughput synthesis, dodecane solutions of cesium oleate (200 x diluted from a Cs-OA stock solution), lead oleate (200 x diluted from a Pb-OA stock solution), benzoyl bromide (80 x diluted - except where noted otherwise), oleylamine (100 x diluted) and oleic acid (80 x diluted) were freshly prepared for every run. Dodecane was chosen as a solvent because of its high boiling

point to prevent evaporation during the reaction and observation, as well as its high optical transparency. Using a Hamilton NIMBUS4 Microlab liquid handling robot, dodecane, oleylamine, lead oleate, oleic acid and cesium oleate solutions were added in varying proportions to a 96 well plate equipped with single-use 1 mL glass vials. The entire plate was heated to the reaction temperature while shaking at 300 rpm and kept at the reaction temperature for 800 s. Under continued shaking, benzoyl bromide solution was added to each vial, for a final reaction volume of 500 μL. This addition sequence was typically performed within 600 s. The plate was kept at the reaction temperature and shaken for another 600 s after the addition.

High-throughput absorption and emission spectra. From a 96-well plate reaction, 30 μL of each 500 μL final reaction solution were removed, diluted with 270 μL dodecane and placed into a 96-well Hellma quartz microreader plate. A Biotek Synergy 4 microplate reader was used to evaluate the reaction solutions. An automatic calibration was carried out before each plate was measured, then absorption spectra were recorded from 250 to 700 nm in 1 nm increments with a single reading per data point, while emission spectra were recorded from 400 to 550 nm in 1 nm increments with an excitation wavelength of 330 nm, with a detector sensitivity of 70 and a single reading per data point.

Post-synthetic reactions. The addition sequence for post synthetic transformation reactions starts in the same fashion as the other high-throughput experiments. After waiting for 600 s upon addition of benzoyl bromide, varying amounts of cesium oleate, lead oleate or oleylamine solution were added while shaking, up to a final reaction volume of 500 μL. Upon addition of the post-synthetic reagents, the reaction plate was shaken for another 600 s before transferal to the microplate for absorption measurements. For every post-synthetic reaction, six vials were prepared with the initial amount of reagents, and three vials were prepared with the final amount of reagents. In three of the six first vials, the difference between initial and final reagent amounts was added after the addition of benzoyl bromide solution, the other three were kept as a reference for the starting material.

Spectral processing and deconvolution. Spectra and reagent amounts were loaded into a pandas dataframe[41]. Spectra that had low absorbance at 250 nm (< 2.5 O.D.) were uniformly discarded, as low absorption in this region indicated a lack of benzoyl bromide addition, except for solutions created with low concentration Br stock solutions. Absorption spectra for references (Figure 3 B) were chosen based on their visual similarity to spectra of phase-pure compounds synthesized by hand (Figure 1), and a single power scattering line (with the power constrained between -4 and 0) was fitted to the 550-700 nm region using the curve_fit algorithm and subtracted from the spectrum. Reference spectra of perovskite species were normalized to the optical density at 310 nm, and other materials were scaled to the same order of

magnitude. We expect the absorption cross section at this wavelength to be mainly dominated by a transition between Pb s and p orbitals under the influence of a bromide coordination environment which should be roughly similar for all of the materials examined here. In addition, one spectrum of background absorption from a vial containing no discernible products as well as scattering lines corresponding to different negative integer power dependencies on the wavelength were added to the references to emulate multiple scattering length scales from the Rayleigh to Mie limits. First and second derivatives of every spectrum with respect to wavelength were calculated after smoothing using a Savitzky-Golay filter[42] as implemented in scipy[43] with a window length of 21 data points and a 4th order polynomial. As the numerical values of the derivatives are smaller than the values of the absorption, the first derivative was weighted 20 times higher and the second derivative was weighted 100 times higher than the original spectrum to yield numerically similar and uniformly increased numbers. A cross-validating LASSO algorithm, LassoCV[44] was used to find the coefficients of best cross-validated fit of the collection of reference spectra and their associated derivatives to every single spectrum and its associated derivatives (Figure 3 A), assigning a penalty value for using reference spectra based on cross validation. These coefficients correspond approximately to the concentration of the respective reference species in the reaction solution, up to a constant extinction coefficient. Fractions of coefficients as well as an R^2 parameter of fit, the final penalty value and the number of iterations were extracted for every spectrum.

Results and Discussion:

Overview. To construct a chemical reaction network, we first need to characterize and confirm the identity of the 9 different reaction products we observe. We then examine an example of transitions between species to see how different variables change the synthesis outcome. To gain a better overview of reaction space, we want to explore the synthesis in an high-throughput fashion, which we accelerate by building an automated deconvolution algorithm which transforms absorption spectra into fractions of different species. Based on the deconvolution, we build a map of synthesis space as a function of Cs, Pb and OLA concentrations. From the map, we can gain insight into the possible reactions occurring during formation and transformation of nanocrystals. We then test these transformation reactions, which helps us determine which of the possible reaction pathways are valid and leads us to the chemical reaction network we describe. Finally, we consider the implications of our model and show that it has significant qualitative explanatory power over previously reported results.

Species Observed in CsPbBr Synthesis Space. We synthesized cesium lead bromide and lead bromide species using a modified version of the method reported by Imran et al.[40] By varying reagent concentrations,

we observed formation of nine species that could be differentiated based on their UV-Vis absorption spectra, and made reference samples to characterize and confirm their identity by UV-Vis absorption, X-ray diffraction and transmission electron microscopy (TEM) (Figure 1). $CsPbBr_3$ nanocubes,[22] nanoplatelets between 1 and 4 lead bromide layers[23,46] and Cs_4PbBr_6[17] have been thoroughly described elsewhere and our results match literature properties. We will describe the properties of $CsPb_2Br_5$, $PbBr_2$ nanocrystals and molecular lead halide species here in more detail, as we have found ambiguities in the literature regarding their characteristics.

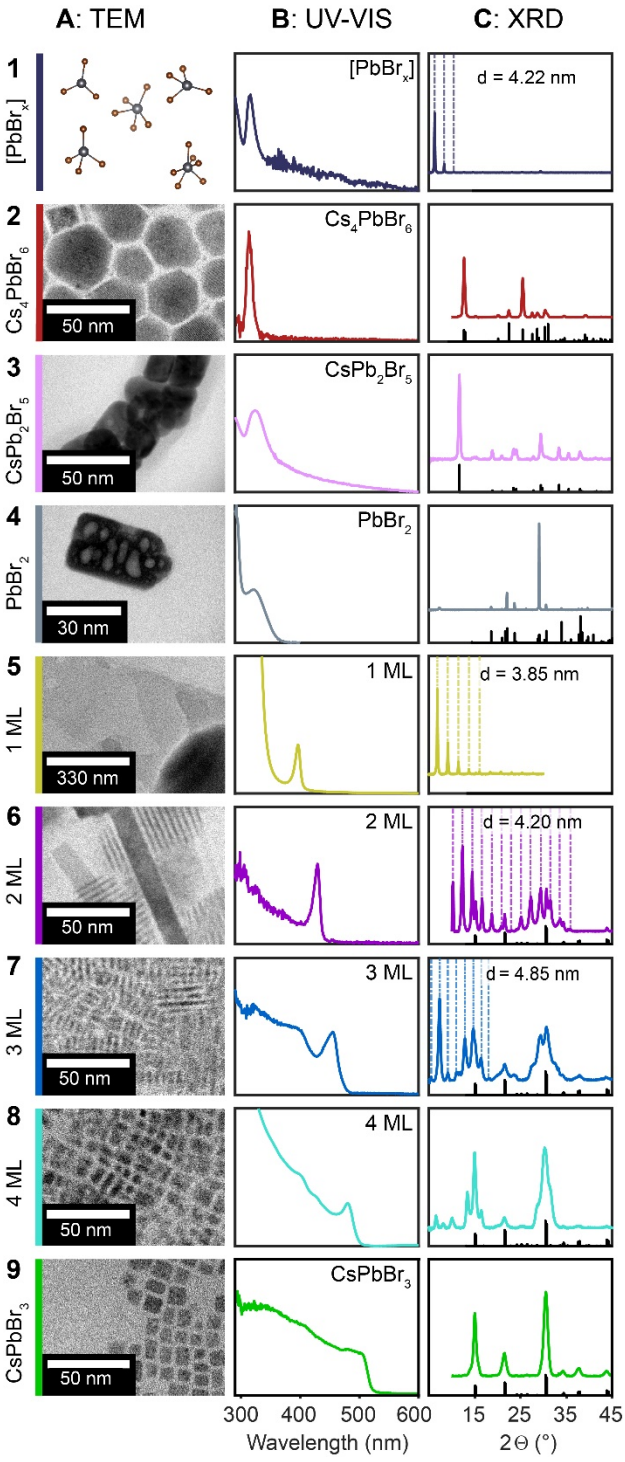

Figure 1. Transmission electron microscopy images (A), absorption spectra (B), and powder X-ray diffraction (C) of the nine species synthesized in this work: (row 1) $[PbBr_x]^{2-x}$ complexes, (2) Cs_4PbBr_6 nanocrystals, (3) $CsPb_2Br_5$ nanocrystals, (3) $PbBr_2$ nanocrystals, (5) OLA_2PbBr_4 nanosheets or 1 monolayer plates (1 ML), (6) $OLA_2CsPb_2Br_7$ nanoplatelets or 2 layer plates (2 ML), (7) $OLA_2Cs_2Pb_3Br_{10}$ nanoplatelets or 3 layer plates (3 ML), (8) $OLA_2Cs_3Pb_4Br_{13}$ nanoplatelets or 4 layer plates (4 ML), (9) $CsPbBr_3$ nanocubes. Vertical axes of (B) and (C) are in arbitrary units and represent absorbance and scattering intensity, respectively. Black sticks in (C) correspond to ICSD reference patterns 162158 (Cs_4PbBr_6), 254290, ($CsPb_2Br_5$), 202134 ($PbBr_2$), 243735 ($CsPbBr_3$). We were unable to image $[PbBr_x]^{2-x}$ species under TEM (1 A).

XRD patterns of $CsPb_2Br_5$ nanocrystals match well with the bulk diffraction pattern[45] (Figure 1 C3). These nanocrystals usually have a clearly observable absorption peak around 320 nm, with onsets starting at 350

nm (Figure 1 B3). This matches data from reflectance spectra of bulk crystals.[45] While we observe photoluminescence from these species (Figure S 2.1 B), it is similar to that of $CsPbBr_3$ species and could easily arise due to small impurities of perovskite cubes or plates in the sample, as has been indicated for the Cs_4PbBr_6 phase.[46]

$PbBr_2$ nanocrystals, as determined by XRD (Figure 1 C2), have a variable absorption onset, occurring between 345 and 370 nm with peaks or shoulders between 330 and 350 nm (Figure 1 B2). This is close to the reflectance spectrum observed for $PbBr_2$ in bulk,[47] and would suggest that nanocrystals observed (Figure 1 A2) do not display strong quantum or dielectric confinement, unlike smaller structures others have prepared.[35,36]

Lead halide complex species can be made by employing a high molar ratio of OLA to Pb-OA of 10:1 and no Cs-OA. We observe an absorption peak at 313 nm in dodecane (Figure 1 B1). If dried, the lead halide species appears to assemble into a layered species, as determined by the characteristic stacking patterns (Figure 1 B2). In previous publications, a lead halide species was reported as $[PbBr_3]^-$ with an absorption peak around 320 nm in polar solvents.[48] The peak we observe in non-polar solvents overlaps almost exactly with the peak of Cs_4PbBr_6, which may lead to confusion of the two species. To distinguish the two spectra, it is necessary to consider the line shape of the two peaks: Cs_4PbBr_6 has a sharper peak with a FWHM of ~10 nm centered around 315 nm, with an onset only starting at 340 nm, while the lead halide complex has broader peak with a FWHM of ~15 nm centered on 313 nm and an onset starting around 350 nm (Figure S 2.8). We further discuss $[PbBr_x]$ species in SI Section 1..

We can confirm the identity of nanocrystalline species through X-ray diffraction patterns, further corroborate these patterns with high-resolution TEM (Figure S 1.5 – S 1.11) and provide a match with their optical absorbance spectra. Given that we observe and differentiate nine species that can be made in this synthesis, we show next how we can go about using this information to understand transitions between different areas of synthetic space.

Transitions Between 2 and 3 Monolayer Nanoplates. A useful example is the transition from 2 to 3 monolayer (ML) platelets (Figure 2). The synthesis outcomes can be observed by the characteristic peaks in optical density at 431 nm (2 ML) and 455 nm (3 ML). Increasing the concentrations of lead oleate and cesium oleate in the synthesis solution will drive a transition from the creation of 2 to 3 layer platelets in this reaction, which can be deduced from the increase in optical density of the peak at 455 nm and decrease of the peak at 431 nm upon increasing reagent concentration. Oleylamine has the opposite effect: increasing concentration leads to higher 2 ML peaks and decreasing concentration leads first to higher 3 ML peaks and then a decrease in the 3 ML peak with a corresponding increase of a 4 ML peak at 473 nm. What is unexpected is the abruptness of this transition: starting at the lower lead and cesium regime or at higher

oleylamine regimes, several reactions produce almost no discernible 3 ML peak. There is a sudden change to conditions producing mostly 3 ML plates, leading to a complete reversal of majority products by the variation of only 10-20 % in the amount of oleylamine and lead, or 50% in the amount of cesium. We also observe that the synthesis becomes more variable close to these transition points (Figure S 2.), with some reactions at ostensibly the same conditions producing more 2-layer plates and other reactions forming mostly 3 layer plates. If this system is non-linear, minute variations in the synthesis conditions due to small errors in addition, dilution or temperature control would strongly influence a reaction close to a critical point and lead to large experimentally observed errors. Reactions performed at conditions that are further from a critical point would be more reproducible. Any effort to create useful maps of the synthetic space must grapple with the shape of this terrain, with areas of relative stability bounded by regions of abrupt change and high variability.

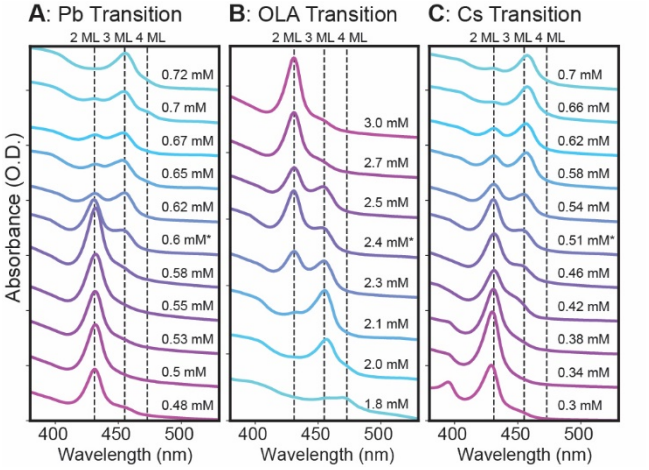

Figure 2. Absorption spectra of as-synthesized solutions of 2 ML and 3 ML nanoplatelets describing a transition point at a Pb-OA concentration ([Pb]) of 0.6 mM, oleylamine concentration ([OLA]) of 2.4 mM, Cs-OA concentration ([Cs]) of 0.51 mM, depending on changes in A) Pb-OA concentration ([OLA] = 2.4 mM, [Cs] = 0.51 mM) B) oleylamine concentration ([Pb] = 0.6 mM, [Cs] = 0.51 mM) and C) Cs-OA concentration ([Pb] = 0.6 mM, [OLA] = 2.4 mM).

Spectral Deconvolution. To systematically investigate the synthetic parameters that result in the formation of the 9 different species, we used our high-throughput workflow to synthesize 2337 samples and measure their absorption spectra. For this large number of reactions, it was crucial to develop an automated method that allowed us to consistently determine the type and approximate amount of each chemical species in the synthesis reaction from absorbance spectra (Figure 3). Our method treats each measured spectrum as a linear combination of reference spectra for each species (Figure 3 C). We used a least absolute shrinkage and selection operator (LASSO[49,50]) constrained to positive values to add penalties for relying on too many

of the reference spectra to fit a measured spectrum, which gave consistent results and restricted the spectra chosen to the majority species in a sample (Figure 3 D).

Fitting values only to the absorption spectra resulted in assignment of species which had no matching peaks in the measured spectrum, and frequently overestimated the amount of $CsPbBr_3$ and larger platelets. Using the first and second derivatives of the absorbance as additional features increased the sensitivity to peak position. The linear combination of reference spectra fit the measured spectra well, with an average R^2 value of 0.976; over 80 % of the spectra have an R^2 value above 0.95 (Figure 3 E). Based on error simulations for this method, we estimate that the fractions of species calculated based on absorbance should be accurate to within 2-3 % of the measured value (Figure S 2.2), unless the fraction itself is below 5% (see SI section 2 for a discussion of simulated and experimental errors). Deconvolution of spectra containing simulated 4 ML and $CsPbBr_3$ absorption exhibited higher errors, with significant underestimates once the fraction of 4 ML or $CsPbBr_3$ was lower than 10 % (Figure S 2.3). This error is significantly smaller than the average experimentally measured variation of 10-25 % absolute error in the measured fractions for repeated nanocrystal synthesis under the same experimental conditions. Larger experimental variations are observed at for a small number of individual points (Figure S 2.4-2.6). Overall, this high-throughput spectral deconvolution allows us to consistently and reproducibly determine the relative amount of the species produced by a synthesis.

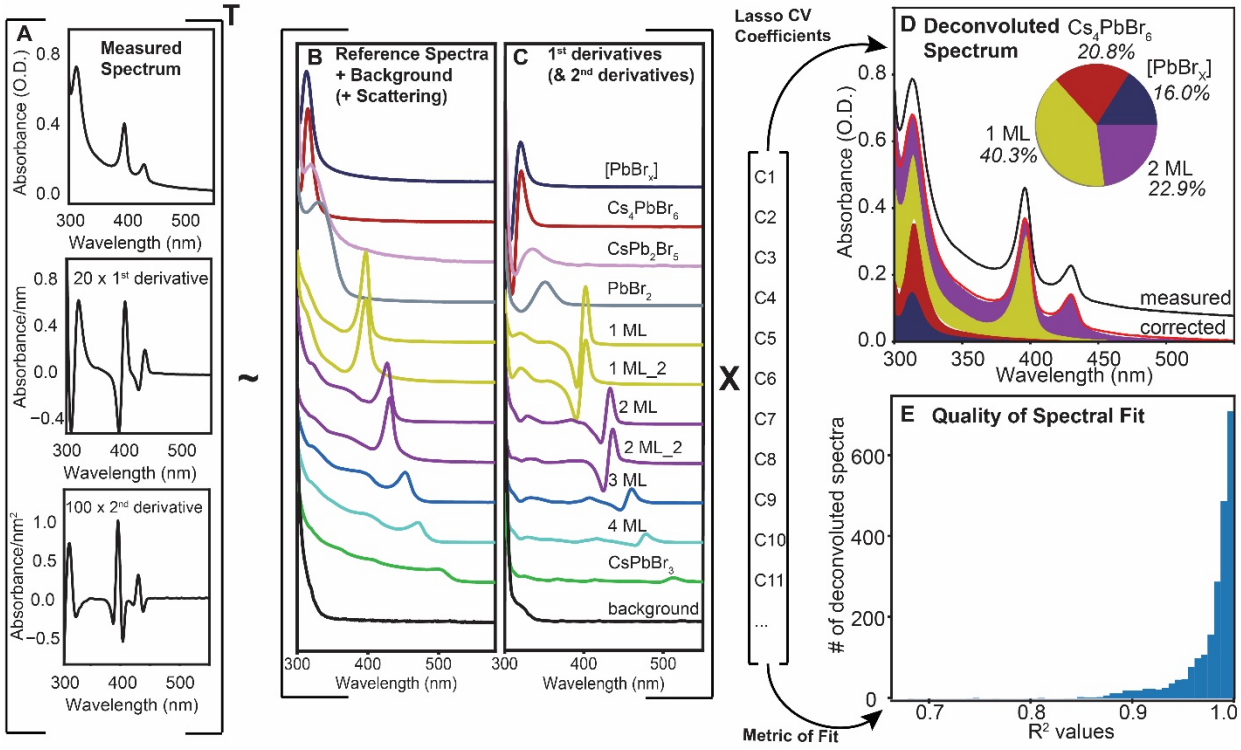

Figure 3. Vector representation of the spectral deconvolution process. An experimentally measured spectrum and its first and second derivatives (A) are deconvoluted using a LASSO algorithm into a linear

combination of eleven reference spectra (B) and their derivatives (C). Deconvoluted example spectrum (D), showing fractional contributions of [$PbBr_x$], Cs_4PbBr_6, 1 ML and 2 ML. (E) Distribution of R^2 values for the fits of the 2337 spectra measured for this work.

High-Throughput Synthesis Map. Having established a method to quantify the distribution of species produced by Cs-Pb-Br nanocrystal reactions, we mapped the formation of those species over a range of Cs-OA, Pb-OA, and OLA concentrations in order to gain a holistic view of synthetic space. Other maps of other variables can be found in section 3 of the SI. We performed synthesis experiments in a factorial expansion across 9 concentrations of cesium precursor (0.0-0.8 mM, in steps of 0.1 mM), 9 concentrations of lead precursor (0.13 to 1.24 mM, 0.12 mM steps) and 6 concentrations of oleylamine (1.2, 1.8, 2.4, 3.0, 3.6 and 4.9 mM) for a total of 486 reactions. Reactions (500 µl) were performed at 30° C, with a concentration of 4.8 mM oleic acid and 12.2 mM benzoyl bromide added to each solution. We construct the synthesis map in Figure 4 from the resulting absorption spectra (Figures S 3.1-3.6) using spectral deconvolution to determine the fraction of each species at each reaction condition (Figure S 3.7). Colors correspond to different products, while contour levels (50 %, 70 % and 90 %) indicate levels of purity by spectral analysis.

To determine the new insight we can extract from this high-throughput dataset, we first consider a broad overview of the map. All nine species shown in Figure 1 can be found at some point in this dataset. In fact, we only identified the $PbBr_2$, [$PbBr_x$] and $CsPb_2Br_5$ species after analyzing spectra that did not fit well during deconvolution. Additionally, the observation of areas of the same color connecting in the map means that similar conditions usually create similar products, which is sensible chemically and supports our assessment that the analysis is accurately detecting the relative amount of different species. This is especially important in cases where the species are spectrally similar, as is the case between lead bromide complexes (dark grey) and Cs_4PbBr_6 (red). The cases in which clear islands appear, such as the 3 ML (blue) island in the 2 ML (purple) cluster in Figure 4 D appear correct in their spectral assignment (Figure S 3.4), are caused by single reactions and are most likely experimental outliers. Domains that persist over a range of variations are robustly identified, but the exact positions of boundaries should be treated with robust skepticism. Future studies with greater precision of dispensing and higher map densities are also surely worth pursuing in order to carefully traverse the boundaries between the domains. Our best judgement is that the current experiments provide no evidence for magic numbers, or one island of a composition that is wholly surrounded by another composition. Overall, the map represents a portion of synthetic space containing all species we are analyzing and shows that those species cluster into areas with similar conditions.

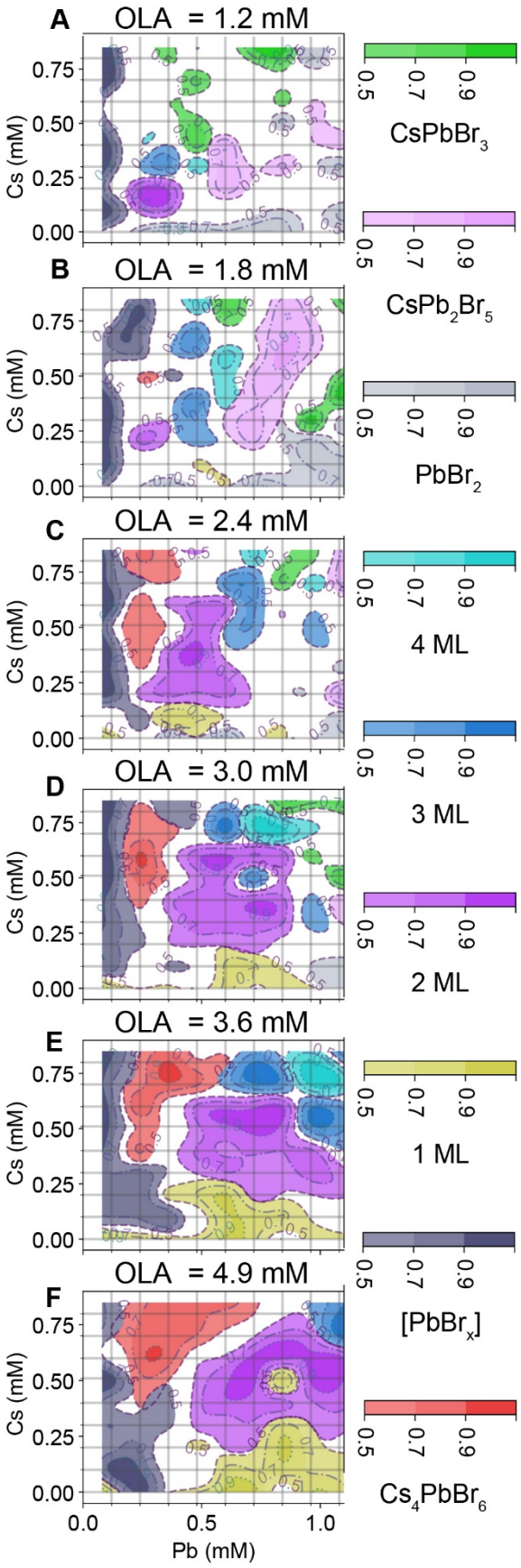

Figure 4. Map of majority species and level of spectral purity depending on the concentration of cesium and lead at oleylamine concentrations of (A) 1.2 mM, (B) 1.8 mM, (C) 2.4 mM, (D) 3.0 mM, (E) 3.6 mM, and (F) 4.9 mM. Reactions were performed at the intersection of the grid lines; areas between are colored via cubic interpolation of all neighboring data points. Colored regions of the map indicate the majority species (species fraction > 0.5), with contour shading defined by color scales on the right. White denotes no majority species.

Considering Potential Reactions based on Positions in Synthetic Space. We now consider specific species and their position in synthetic space. We will use this information to learn how Cs, Pb and OLA precursor concentrations tune synthetic pathways and construct hypothesis of reaction pathways to test. The distribution of perovskite species is consistent with previous reports of Pb/OLA[29] ratios or Cs/OLA[26] ratios controlling the reaction outcome. Nanocrystals of lead-rich ($CsPb_2Br_5$) and lead-depleted (Cs_4PbBr_6) phases appear towards the right side (high Pb) and upper side (high Cs) of Figure 4, respectively, as would be expected from their stoichiometry. The role of OLA in the formation of Cs_4PbBr_6 matches with that previously reported, with higher [OLA] leading to more Cs_4PbBr_6,[26] as does the role of the Cs/Pb ratio[30]. The synthesis of $CsPb_2Br_5$ has not been explored similarly to date. We observe that nanocrystals with $CsPb_2Br_5$ phase form at high [Pb] and low [Cs], which would be expected based on the lead-rich stoichiometry. The formation of $CsPb_2Br_5$ at lower [OLA] is unexpected, however. As there is no obvious incorporation of oleylamine into either Cs_4PbBr_6 or $CsPb_2Br_5$ or clear surface stabilization, this suggests that oleylamine is likely important in the formation processes.

We next consider the areas of the map that contain the binary lead bromide species to understand how they fit into this synthetic space. Perhaps the most surprising result of this map is that at the lowest [Pb], there is always lead bromide complex present irrespective of the amount of Cs-OA in solution. With increasing amounts of oleylamine, the region occupied by the lead bromide complex expands to higher lead concentrations, except at high Cs concentrations where the Cs_4PbBr_6 phase will form. Regions containing $PbBr_2$ nanocrystals or OLA_2PbBr_4 nanosheets are confined mainly to the low [Cs] regime, as would be expected for binary lead bromide phases. In general, $PbBr_2$ is the major species at low levels of OLA while the nanosheets dominate at high [OLA]. The concentration of lead plays a role at intermediate [OLA], with higher concentrations of lead leading to formation of more $PbBr_2$. As the binary lead halide species occupy all of the synthetic space at the lowest inorganic component concentrations, it is quite likely that they play key roles in the formation process of all of the ternary compounds, as for the formation of nanocrystals we would need to pass through those areas of low inorganic component concentrations to achieve the higher concentrations required for crystallite nucleation.

Considering the concept of passing through lower inorganic component concentrations to reach regions with higher inorganic component concentrations during synthesis, we examine which species are most often found next to each binary lead bromide species. $PbBr_2$ is adjacent to regions containing $CsPb_2Br_5$, and in most regions containing $CsPbBr_3$ at lower Cs concentrations. 1 ML are connected to $PbBr_2$ at higher OLA concentrations or lower Pb concentrations. These single layer plates are in turn almost always adjacent to bilayer plates at higher Cs concentrations. The lead bromide complex is found next to all perovskite phases, the Cs_4PbBr_6 phase and the monolayer plates at lower Pb concentrations, and adjacent to the Cs_4PbBr_6 at lower Cs concentrations. Multiple potential pathways towards product formation now

become apparent, depending on whether products form based on direct nucleation from lead halide complexes, from transformation of the other lead halide species or through dissolution and reprecipitation. Moving to the interactions of the ternary phases, the set of 2-, 3- and 4-layer plates and nanocubes are lined up in that order along a series of increasing Cs or Pb values, or decreasing OLA values, which suggests a potential island nucleation mediated layer growth pathway of the plates as in II-VI nanocrystals. Larger plates and nanocubes are adjacent to the $CsPb_2Br_5$ phase at higher Pb values, and sometimes at lower Cs values, which could potentially be explained through transformations of the $CsPb_2Br_5$ and the $CsPbBr_3$ phases. Majority Cs_4PbBr_6 areas appear to be adjacent only to the 2 and 3 ML plates at lower Pb values, though there is some formation of Cs_4PbBr_6 at lower Pb values in areas containing any perovskite. Overall, the synthesis map suggests many possible reactions that we can group into multiple possible pathways towards formation of different products and nanocrystal transformation processes.

Testing Reaction Pathways through Chemical Transformations. While the adjacency of two species in synthetic space can help us construct hypothetical reaction pathways, it is not clear that the chemical transformation between the two species occurs - and if so whether it is reversible or irreversible. This is crucial to determine which of the potential pathways are relevant in nanocrystal transformation and formation reactions. To probe this directly, we used the map to find sets of two points in which the majority species changes by slightly varying the concentration of only one species. We then attempt to transform one of these species into the other by adding Cs-OA, OLA or Pb-OA after the reaction was initiated by halide precursor injection to see which of the possible reactions exist. By examining the reactions which exist, we can also understand which reactions are reversible due to the presence of forward and inverse reactions. Figure 5 A and B describe this process by showcasing four examples of chemical transformations. In Figure 5A, a solution containing $PbBr_2$ nanocrystals can be transformed into $CsPbBr_3$ by adding Cs-OA, or into a solution containing 1 ML plates by adding OLA. The two transformations have very similar results to the direct synthesis, suggesting that there is a reaction pathway from $PbBr_2$ to these species that is not much different to the formation in the synthesis reaction. In Figure 5B, a solution containing 1 ML plates is transformed into $PbBr_2$ by adding Pb-OA or into a mixture of 2 ML plates by adding Cs-OA. The transformation into lead bromide appears facile, whereas the transformation into the nanoplates appears much more complicated. Compared to the initially synthesized sample, most of the 1 ML plate peak remains in the sample after Cs-OA addition, a small amount of 2 ML plates is formed, and no 3 ML plates appear at all. From this information, we can deduce that there is an equilibrium between $PbBr_2$ and 1 ML, a pathway from $PbBr_2$ to $CsPbBr_3$ and a partial reaction from 1 ML to 2 ML, whereas the reaction from 1 ML to 3 ML does not occur.

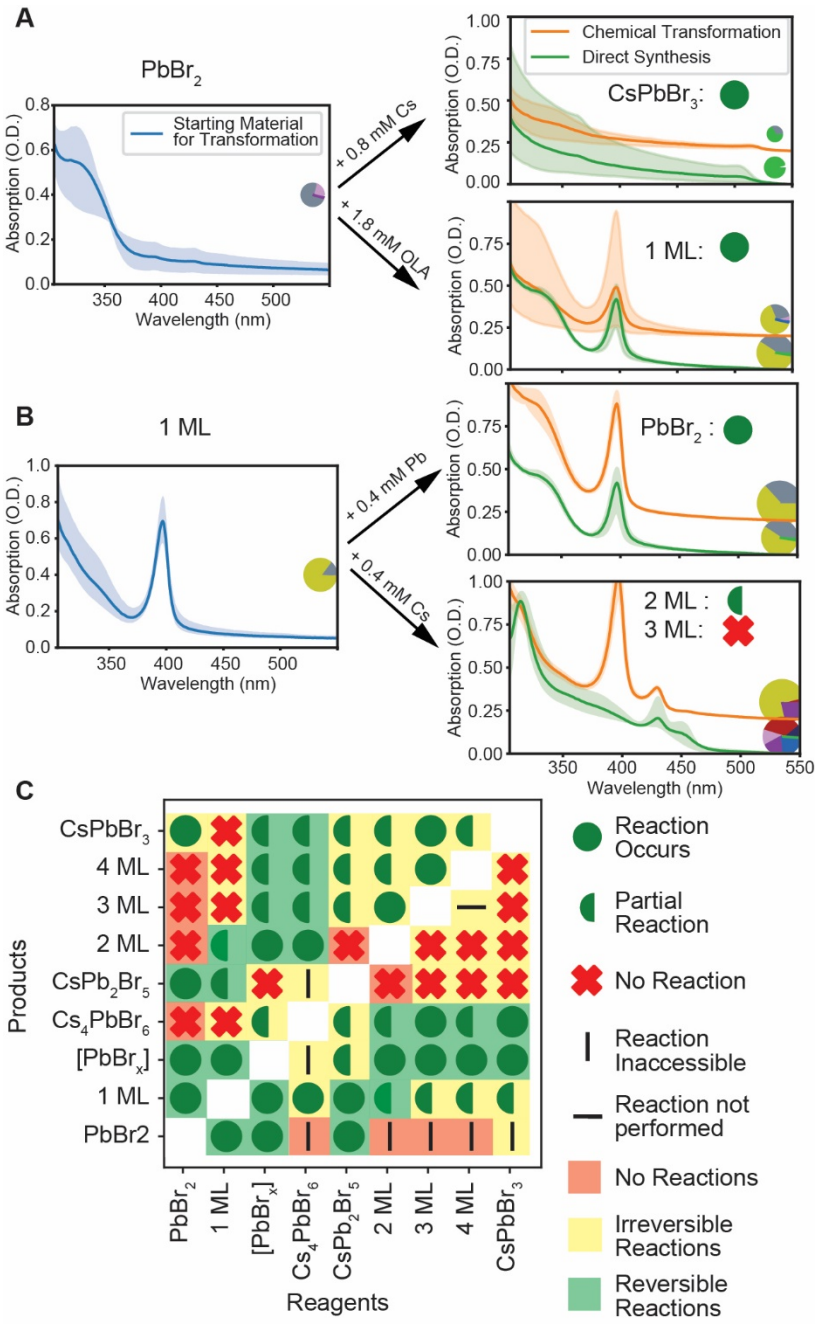

Figure 5. Chemical transformations between species in the Cs-Pb-Br reaction network. (A) Successful transformations of $PbBr_2$ nanocrystals (right) into $CsPbBr_3$ (upper left) through addition of 0.8 mM Cs-OA and into 1 ML nanosheets (lower left) through addition of 18 mM oleylamine. (B) Successful transformation of 1 ML (right) into a mixture of 1 ML and $PbBr_2$ nanocrystals through addition of 0.4 mM Pb-OA (upper left) and mixed results from a transformation into a mixture of 2 ML (partially successful) and 3 ML (unsuccessful) through addition of 0.4 mM Cs-OA. (C) Matrix classifying all pairs of transformations by observed outcome. Inaccessible reactions are transformations in which there is no possible single reagent route from the reagent species to the product species in the parameter space given

by the map in Figure 4. Reversible reactions correspond to both possible reactions being observed, irreversible reactions correspond to one of the two possible reactions observed.

We examine the outcome of 149 transformation reactions, focusing on which interactions suggested from the map are real reactions (Spectral data and additional explanation can be found in Section 4 of the SI). Figure 5 C summarizes the outcomes of all reactions performed, allowing us to constrain possible formation and transformation sequences. For the binary lead bromide species, all forward and inverse transformations are possible through either addition of oleylamine or lead. Presence of forward and inverse reactions implies the existence of a reversible equilibrium between the lead halide nanocrystal, monolayer and complex species. As we remarked previously, the formation of nanocrystals likely proceeds through at least one of these binary lead halide phases. The equilibrium between the binary lead bromide species provides a platform that enables switching between different potential pathways depending on the synthesis conditions.

We now examine what reactions are possible when moving towards the ternary species by adding Cs-OA. $PbBr_2$ can be transformed to $CsPb_2Br_5$ and to large $CsPbBr_3$ crystals, but not to the 2-4 ML platelets or Cs_4PbBr_6. 1 ML platelets can only be partially transformed to 2 ML platelets, but not to larger platelets, cubes or the other ternary phases. As no cesium is present in the initial solution, it is not possible for 2 ML nuclei with a stoichiometry of $OLA_2CsPb_2Br_7$ to form before Cs injection. This may suggest that the strict limitation to Ostwald ripening growth of 2 D nanoplatelets through island nucleation mediated growth shown for II-VI semiconductors[51–53] may be relaxed in the $CsPbBr_3$ system and that growth in the confinement direction may occur, though it is likely to be a rare event. The only species accessible from the lead halide complex through adding Cs is Cs_4PbBr_6 at high OLA concentrations, which is confirmed by chemical transformation as well as an independent study published after this article was posted as a pre-print.[54] If additional lead is administered to a solution containing lead bromide complex in which some Cs is already present, full transformation to Cs_4PbBr_6 and 2 ML plates as well as partial transformation to larger perovskite products is observed. The partial transformation to larger perovskite products is intriguing: instead of forming one or two of the platelet phases as is observed in direct synthesis, adding lead to a solution containing lead bromide complex and cesium induces formation of all the perovskite species (2 ML, 3 ML, 4 ML plates and nanocubes) as well as the single monolayer plate in the same reaction solution. This suggests that the process of forming the nanoplatelets is changed when starting from a solution containing Cs and the lead halide complex, as opposed to a halide free solution. This observation has significant implications for the development of a holistic picture of the synthesis of cesium lead halide nanocrystals, as it suggests that lead bromide complexes are not the most direct intermediates on the way to formation of perovskite species.

Let us finally examine transformations among the ternary species to further elucidate growth and transformation reactions. It is possible to transform a thinner nanoplate into a thicker one or a nanocube by adding lead or cesium, but it is not possible to transform a thick nanoplate into a thin nanoplate. Instead, adding oleylamine to perovskite species results in the formation of lead halide complex, Cs_4PbBr_6 (as reported in a series of previous work[19,20]), and single layer nanosheets. Transformation into $PbBr_2$ or $CsPb_2Br_5$ also appears suppressed. The ubiquitous presence of lead halide complex in reactions in which OLA was added to the solution adds further credence to the dissolution-reprecipitation processes proposed for the transformation between perovskites and other ternary phases.[20,21] The Cs_4PbBr_6 phase appears to react quite similarly to the lead bromide complex concerning the reactions producing the perovskite phases, producing the entire array of perovskite species when lead is added, suggesting the possibility that the two phases may share reaction pathways. However, it does not appear to have a ready transformation towards $PbBr_2$, mainly due to its location on the opposite side of synthetic space.

Chemical Reaction Network

Integrating these observations into a diagram of cesium lead bromide nanoparticle formation leads us to Scheme 1. In our interpretation, the most important concept is the mutual equilibrium of lead halide species at the top of the diagram, with $PbBr_2$ nanocrystals, single monolayer plates and lead bromide complexes interconverting. This equilibrium is a uniquely determining factor in the reaction because of the different reactions each of the species may take when exposed to cesium: $PbBr_2$ reacts with cesium to form either nanocubes or $CsPb_2Br_5$, whereas the monolayer plate will react to form a 2 layer plate and the molecular complex will form Cs_4PbBr_6. The platelets appear to grow irreversibly one layer at a time, which could be explained both by island nucleation mediated layer growth in the confinement direction as suggested by the transformation of 1 ML to 2 ML plates or nucleation of larger cores and subsequent layer dependent Ostwald ripening as in II-VI nanoplatelets.[52] All phases can be decomposed into lead bromide complex, which can then react to Cs_4PbBr_6 and lead bromide monolayers and nanocrystals, enabling dissolution-reprecipitation processes for all transformations between cesium lead bromide nanocrystals.

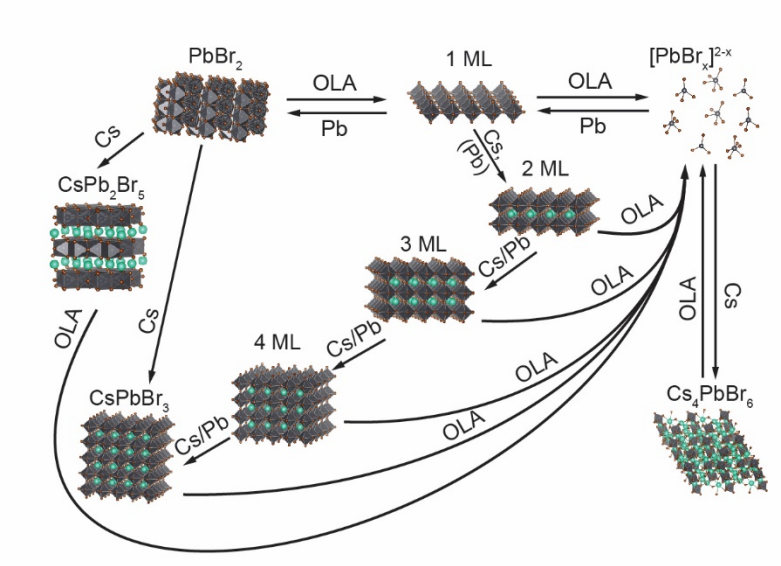

Scheme 1. Chemical reaction network diagram of $Cs_xPb_yBr_z$ nanocrystals.

Now that we have obtained an overall reaction diagram, let us examine what information we can learn from its structure. The connectivity of the reaction diagram suggests the existence of a multi-component reaction network as the basis of the $CsPbBr_3$ formation reaction. While not all the reactions shown here are reversible, the reaction network allows any species to be converted to any other species if the appropriate path through the network is taken. This property of a network is known as weak reversibility to mathematicians studying chemical reaction network theory.[55] To chemists, weak reversibility may offer an explanation for why certain reactions, such as the transformation of perovskite nanocrystals to Cs_4PbBr_6 or $CsPb_2Br_5$ can sometimes take days even though all crystals can be formed and dissolved rapidly at room temperature. The reactions that take longer must proceed over several intermediates, any of which might only be present in miniscule amounts, thus reducing the overall speed of transformation drastically even if each individual reaction is facile. Another important result of thinking of this synthesis in terms of a reaction network is allowing for non-linear changes in product amounts despite linear variations of the input: Critical points and non-linear transitions from one species to the next frequently arise when multiple reactions are coupled with each other, even if each reaction is linear. This can qualitatively explain the sudden transitions between chemical species, such as in the perovskite nanoplatelets. It also explains why it is usually quite easy to create 2 and 3 layer species in a phase-pure manner, while larger species are often found in mixtures. Overall, the reaction network structure provides concepts that help explain some of the peculiar chemical properties observed in this nanocrystal system, such as reversible ligand-induced phase transformation and critical points in the production of several products.

Explaining Previous Results with the Chemical Reaction Network. We now consider the effect of the chemical reaction network on $CsPbBr_3$ synthesis. There are two formation pathways of $CsPbBr_3$ species, and they are modulated through an equilibrium of the intermediate lead bromide species. We discuss previously reported nanocrystal synthesis results to provide further context and to test the explanatory power of the chemical model developed. Due to the presence of lead, bromide and oleylammonium ions in solution, syntheses derived from the method of Protesescu et al.[22] may be considered a transformation from different binary lead halide species in solution to ternary phases upon addition of Cs. Our reaction network can explain the results of temperature control in this method, which induces formation of thin nanoplates at 90 °C,[23] thicker nanoplates at 130 °C, small nanocubes at 160 °C[22] and larger nanocrystals at 200 °C. We see similar effects shifting the areas where plates and cubes are formed at lower temperatures and with the different synthetic method we employ (Figure S 3.11). The transition from platelets to cubes is easy to explain in terms of relative amounts of $PbBr_2$ and OLA_2PbBr_4 in equilibrium leading to different reaction pathways and products. However, if there is truly a dynamic equilibrium between these two species, it should also influence the crystallite size, which is likely to influence the size of species after transformation. If conditions strongly favor one side of the equilibrium, crystals of that species are unlikely to ever dissolve fully and as a result, particle sizes are likely to be larger. In a balanced dynamic equilibrium state, we would expect rapid formation and dissolution of crystals of both species, leading to overall smaller crystallite sizes. We see evidence of this difference in size as a function of equilibrium control in blue shifts of absorption spectra for 1 ML plates at lower OLA concentrations (Figure 6 A) and $PbBr_2$ at higher OLA concentrations (Figure 6 B). For $PbBr_2$, smaller crystal sizes before Cs intercalation would lead to smaller perovskite cubes, and larger crystals would lead to larger cubes. For monolayer lead bromide, a larger crystal size means a larger lateral size, since without cesium, this layered compound is confined in one dimension. Research examining the growth of CdSe nanoplatelets[51] suggests that under conditions of layer-by-layer growth on an anisotropic nanocrystal, a larger lateral size would decrease growth in the confinement dimension. If this is the case, smaller monolayer crystals would lead to thicker platelets and larger monolayer sheets will grow into thinner platelets, explaining the transition from thin plates to thick plates to small cubes to large cubes seen with temperature and other variables controlling the equilibrium between OLA_2PbBr_4 and $PbBr_2$ nanostructures (Figure 6 C).

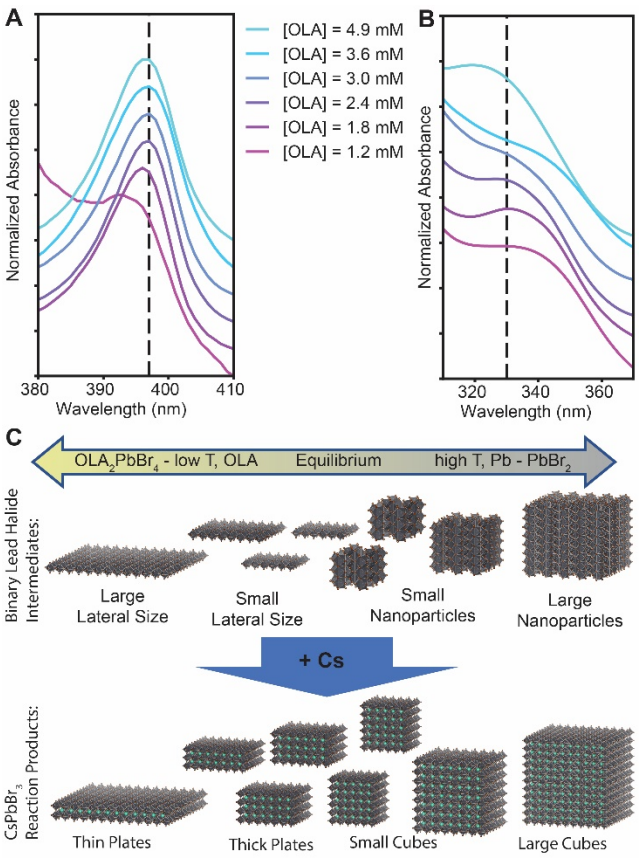

Figure 6. A) Spectra of OLA_2PbBr_4 nanosheets (1 ML plates) at varying concentrations of oleylamine. [Cs] = 0, [Pb] = 0.13 mM, [Br] =12.9 mM, [OA] = 5.4 mM. B) Spectra of $PbBr_2$ nanocrystals at varying concentrations of oleylamine. [Cs] = 0, [Pb] = 0.92 mM, [Br] =12.9 mM, [OA] = 9.2 mM. C) Scheme showing the proposed effect of the equilibrium between OLA_2PbBr_4 nanosheets and $PbBr_2$ nanocrystals on the size and shape of reaction intermediates and on perovskite nanoplates and cubes.

We thus show that the model we have built allows us to transfer knowledge from our synthesis study to other methods as well as explaining additional properties such as size control that were initially not examined, demonstrating the qualitative explanatory power of our results (further discussion in SI section 5). We believe that expanding the knowledge of dynamic processes in this complicated nanocrystal system provides a new frontier for increasing and refining our understanding of nanocrystal formation and transformation reactions.

Conclusion:

In this work, we use quantitative and qualitative analysis of high-throughput synthesis data to determine a cohesive chemical reaction network for lead halide and cesium lead halide nanocrystals. This is

accomplished through combining factorial exploration of synthesis space and an automated method for deconvoluting absorption spectra to create maps and transformations. We find that this nanocrystal reaction network is weakly reversible, which helps explain the equilibria observed between nanocrystal species of different phases. The reaction is largely determined by an equilibrium between lead bromide nanocrystals, monolayers and complexes. We examine previously published experiments through the lens of our model and find that our reaction network has substantial qualitative explanatory power. This work can offer a cohesive understanding of the formation and transformation reactions of cesium lead halide nanocrystals. Furthermore, our combination of quantitative mapping and qualitative transformation experiments allows us to gain a holistic view of the reaction that is helpful for developing understanding. The work presented here also suggests that further combinations of high throughput tools with data science approaches can be productive in deciphering reaction networks that govern the synthesis of nanomaterials. We believe this approach could be transferred to other complex chemical systems where an interplay of kinetic and thermodynamic factors complicates the outcomes.

Acknowledgements:

This work was supported by the U.S. Department of Energy, Office of Science, Office of Basic Energy Sciences, Materials Sciences and Engineering Division, under Contract No. DE-AC02-05-CH11231 within the Physical Chemistry of Inorganic Nanostructures Program (KC3103). Work at the Molecular Foundry was supported by the Office of Science, Office of Basic Energy Sciences, of the U.S. Department of Energy under Contract No. DE-AC02-05CH11231. J.C.D. acknowledges support by the National Science Foundation Graduate Research Fellowship under DGE 1752814 and by the Kavli NanoScience Institute, University of California, Berkeley through the Philomathia Graduate Student Fellowship. We thank Dr. Samuel Niblett, Dr. Justin Ondry and Dr. Brent Kosher for providing insightful review of the manuscript. We would also like to thank Prof. David Limmer, Dr. Anubhav Jain, Dr. Yehonadav Bekenstein, Prof. Jennifer Listgarten, Dr. Assaf Ben-Moshe, Dr. Ayelet Teitelboim, Dr. Zhi Li, Dr. Ivan Moreno-Hernandez, Dr. David Nenon, Dr. Joseph Swabeck, Dr. David Hanifi, Dr. Dmitry Baranov, Abdullah Abbas, Samuel Gleason and QinQin Yu for insightful discussions concerning this project, as well as our group-based undergraduate research program students from the 2019 and 2020 robotics section for inspiration.

Supporting Information

Supporting Information.pdf: Additional information on the synthesis, HR TEM images, data collection procedures, helpful visualizations and information on the chemical transformations, further discussion.

Dataset published on Dryad as: Dahl, Jakob; Wang, Xingzhi; Chan, Emory; Alivisatos, Paul (2020), Cesium lead bromide nanocrystal high-throughput synthesis mapping and transformation experiments, UC Berkeley, Dataset, https://doi.org/10.6078/D1XT4F.

Author Information:
Corresponding Author:
*paul.alivisatos@berkeley.edu

The authors declare no conflicts of interest

References

(1) Gromski, P. S.; Henson, A. B.; Granda, J. M.; Cronin, L. How to Explore Chemical Space Using Algorithms and Automation. *Nat. Rev. Chem.* **2019**, *3*, 119–128.

(2) Stokes, J. M.; Yang, K.; Swanson, K.; Jin, W.; Cubillos-Ruiz, A.; Donghia, N. M.; MacNair, C. R.; French, S.; Carfrae, L. A.; Bloom-Ackerman, Z.; et al. A Deep Learning Approach to Antibiotic Discovery. *Cell* **2020**, *180*, 688-702.e13.

(3) Troshin, K.; Hartwig, J. F. Snap Deconvolution: An Informatics Approach to High-Throughput Discovery of Catalytic Reactions. *Science (80-.).* **2017**, *357*, 175–181.

(4) Ahneman, D. T.; Estrada, J. G.; Lin, S.; Dreher, S. D.; Doyle, A. G. Predicting Reaction Performance in C–N Cross-Coupling Using Machine Learning. *Science (80-.).* **2018**, *360*, 186–190.

(5) Raccuglia, P.; Elbert, K. C.; Adler, P. D. F.; Falk, C.; Wenny, M. B.; Mollo, A.; Zeller, M.; Friedler, S. A.; Schrier, J.; Norquist, A. J. Machine-Learning-Assisted Materials Discovery Using Failed Experiments. *Nature* **2016**, *533*, 73–76.

(6) Potyrailo, R.; Rajan, K.; Stoewe, K.; Takeuchi, I.; Chisholm, B.; Lam, H. Combinatorial and High-Throughput Screening of Materials Libraries: Review of State of the Art. *ACS Comb. Sci.* **2011**, *13*, 579–633.

(7) Xia, Y.; Xiong, Y.; Lim, B.; Skrabalak, S. E. Shape-Controlled Synthesis of Metal Nanocrystals: Simple Chemistry Meets Complex Physics? *Angew. Chemie Int. Ed.* **2009**, *48*, 60–103.

(8) Cui, J.; Chu, Y. S.; Famodu, O. O.; Furuya, Y.; Hattrick-Simpers, J.; James, R. D.; Ludwig, A.; Thienhaus, S.; Wuttig, M.; Zhang, Z.; et al. Combinatorial Search of Thermoelastic Shape-Memory Alloys with Extremely Small Hysteresis Width. *Nat. Mater.* **2006**, *5*, 286–290.

(9) Langille, M. R.; Personick, M. L.; Zhang, J.; Mirkin, C. A. Defining Rules for the Shape Evolution of Gold Nanoparticles. *J. Am. Chem. Soc.* **2012**, *134*, 14542–14554.

(10) Owen, J. S.; Park, J.; Trudeau, P.-E.; Alivisatos, A. P. Reaction Chemistry and Ligand Exchange at Cadmium−Selenide Nanocrystal Surfaces. *J. Am. Chem. Soc.* **2008**, *130*, 12279–12281.

(11) Owen, J. S.; Chan, E. M.; Liu, H.; Alivisatos, A. P. Precursor Conversion Kinetics and the Nucleation of Cadmium Selenide Nanocrystals. *J. Am. Chem. Soc.* **2010**, *132*, 18206–18213.

(12) Gary, D. C.; Terban, M. W.; Billinge, S. J. L.; Cossairt, B. M. Two-Step Nucleation and Growth of InP Quantum Dots via Magic-Sized Cluster Intermediates. *Chem. Mater.* **2015**, *27*, 1432–1441.

(13) Chan, E. M.; Xu, C.; Mao, A. W.; Han, G.; Owen, J. S.; Cohen, B. E.; Milliron, D. J. Reproducible, High-Throughput Synthesis of Colloidal Nanocrystals for Optimization in Multidimensional Parameter Space. *Nano Lett.* **2010**, *10*, 1874–1885.

(14) Berry, J.; Buonassisi, T.; Egger, D. A.; Hodes, G.; Kronik, L.; Loo, Y.-L.; Lubomirsky, I.; Marder, S. R.; Mastai, Y.; Miller, J. S.; et al. Hybrid Organic-Inorganic Perovskites (HOIPs): Opportunities and Challenges. *Adv. Mater.* **2015**, *27*, 5102–5112.

(15) Saparov, B.; Mitzi, D. B. Organic–Inorganic Perovskites: Structural Versatility for Functional Materials Design. *Chem. Rev.* **2016**, *116*, 4558–4596.

(16) Stranks, S. D.; Snaith, H. J. Metal-Halide Perovskites for Photovoltaic and Light-Emitting Devices. *Nat. Nanotechnol.* **2015**, *10*, 391–402.

(17) Akkerman, Q. A.; Park, S.; Radicchi, E.; Nunzi, F.; Mosconi, E.; De Angelis, F.; Brescia, R.; Rastogi, P.; Prato, M.; Manna, L. Nearly Monodisperse Insulator Cs4PbX6 (X = Cl, Br, I) Nanocrystals, Their Mixed Halide Compositions, and Their Transformation into CsPbX3 Nanocrystals. *Nano Lett.* **2017**, *17*, 1924–1930.

(18) Wang, K.-H.; Wu, L.; Li, L.; Yao, H.-B.; Qian, H.-S.; Yu, S.-H. Large-Scale Synthesis of Highly Luminescent Perovskite-Related CsPb 2 Br 5 Nanoplatelets and Their Fast Anion Exchange. *Angew. Chemie Int. Ed.* **2016**, *55*, 8328–8332.

(19) Liu, Z.; Bekenstein, Y.; Ye, X.; Nguyen, S. C.; Swabeck, J.; Zhang, D.; Lee, S. T.; Yang, P.; Ma, W.; Alivisatos, A. P. Ligand Mediated Transformation of Cesium Lead Bromide Perovskite Nanocrystals to Lead Depleted Cs4PbBr6 Nanocrystals. *J. Am. Chem. Soc.* **2017**, *139*, 5309–5312.

(20) Udayabhaskararao, T.; Houben, L.; Cohen, H.; Menahem, M.; Pinkas, I.; Avram, L.; Wolf, T.; Teitelboim, A.; Leskes, M.; Yaffe, O.; et al. A Mechanistic Study of Phase Transformation in Perovskite Nanocrystals Driven by Ligand Passivation. *Chem. Mater.* **2018**, *30*, 84–93.

(21) Balakrishnan, S. K.; Kamat, P. V. Ligand Assisted Transformation of Cubic CsPbBr 3 Nanocrystals into Two-Dimensional CsPb 2 Br 5 Nanosheets. *Chem. Mater.* **2018**, *30*, 74–78.

(22) Protesescu, L.; Yakunin, S.; Bodnarchuk, M. I.; Krieg, F.; Caputo, R.; Hendon, C. H.; Yang, R. X.; Walsh, A.; Kovalenko, M. V. Nanocrystals of Cesium Lead Halide Perovskites (CsPbX3, X = Cl, Br, and I): Novel Optoelectronic Materials Showing Bright Emission with Wide Color Gamut.

Nano Lett. **2015**, *15*, 3692–3696.

(23) Bekenstein, Y.; Koscher, B. A.; Eaton, S. W.; Yang, P.; Alivisatos, A. P. Highly Luminescent Colloidal Nanoplates of Perovskite Cesium Lead Halide and Their Oriented Assemblies. *J. Am. Chem. Soc.* **2015**, *137*, 16008–16011.

(24) Yassitepe, E.; Yang, Z.; Voznyy, O.; Kim, Y.; Walters, G.; Castañeda, J. A.; Kanjanaboos, P.; Yuan, M.; Gong, X.; Fan, F.; et al. Amine-Free Synthesis of Cesium Lead Halide Perovskite Quantum Dots for Efficient Light-Emitting Diodes. *Adv. Funct. Mater.* **2016**, *26*, 8757–8763.

(25) Pan, A.; He, B.; Fan, X.; Liu, Z.; Urban, J. J.; Alivisatos, A. P.; He, L.; Liu, Y. Insight into the Ligand-Mediated Synthesis of Colloidal CsPbBr 3 Perovskite Nanocrystals: The Role of Organic Acid, Base, and Cesium Precursors. *ACS Nano* **2016**, *10*, 7943–7954.

(26) Almeida, G.; Goldoni, L.; Akkerman, Q.; Dang, Z.; Khan, A. H.; Marras, S.; Moreels, I.; Manna, L. Role of Acid–Base Equilibria in the Size, Shape, and Phase Control of Cesium Lead Bromide Nanocrystals. *ACS Nano* **2018**, *12*, 1704–1711.

(27) Imran, M.; Ijaz, P.; Baranov, D.; Goldoni, L.; Petralanda, U.; Akkerman, Q.; Abdelhady, A. L.; Prato, M.; Bianchini, P.; Infante, I.; et al. Shape-Pure, Nearly Monodispersed CsPbBr 3 Nanocubes Prepared Using Secondary Aliphatic Amines. *Nano Lett.* **2018**, *18*, 7822–7831.

(28) Sun, S.; Yuan, D.; Xu, Y.; Wang, A.; Deng, Z. Ligand-Mediated Synthesis of Shape-Controlled Cesium Lead Halide Perovskite Nanocrystals via Reprecipitation Process at Room Temperature. *ACS Nano* **2016**, *10*, 3648–3657.

(29) Braham, E. J.; Cho, J.; Forlano, K. M.; Watson, D. F.; Arròyave, R.; Banerjee, S. Machine Learning-Directed Navigation of Synthetic Design Space: A Statistical Learning Approach to Controlling the Synthesis of Perovskite Halide Nanoplatelets in the Quantum-Confined Regime. *Chem. Mater.* **2019**, *31*, 3281–3292.

(30) Jing, Q.; Xu, Y.; Su, Y.; Xing, X.; Lu, Z. A Systematic Study of the Synthesis of Cesium Lead Halide Nanocrystals: Does Cs 4 PbBr 6 or CsPbBr 3 Form? *Nanoscale* **2019**, *11*, 1784–1789.

(31) Sichert, J. A.; Tong, Y.; Mutz, N.; Vollmer, M.; Fischer, S.; Milowska, K. Z.; García Cortadella, R.; Nickel, B.; Cardenas-Daw, C.; Stolarczyk, J. K.; et al. Quantum Size Effect in Organometal Halide Perovskite Nanoplatelets. *Nano Lett.* **2015**, *15*, 6521–6527.

(32) Koscher, B. A.; Nett, Z.; Alivisatos, A. P. The Underlying Chemical Mechanism of Selective Chemical Etching in CsPbBr 3 Nanocrystals for Reliably Accessing Near-Unity Emitters. *ACS Nano* **2019**, *13*, 11825–11833.

(33) Palazon, F.; Urso, C.; De Trizio, L.; Akkerman, Q.; Marras, S.; Locardi, F.; Nelli, I.; Ferretti, M.; Prato, M.; Manna, L. Postsynthesis Transformation of Insulating Cs 4 PbBr 6 Nanocrystals into Bright Perovskite CsPbBr 3 through Physical and Chemical Extraction of CsBr. *ACS Energy Lett.*

2017, *2*, 2445–2448.

(34) Wen, J.-R.; Roman, B. J.; Rodriguez Ortiz, F. A.; Mireles Villegas, N.; Porcellino, N.; Sheldon, M. Chemical Availability of Bromide Dictates CsPbBr 3 Nanocrystal Growth. *Chem. Mater.* **2019**, *31*, 8551–8557.

(35) Hassan, Y.; Song, Y.; Pensack, R. D.; Abdelrahman, A. I.; Kobayashi, Y.; Winnik, M. A.; Scholes, G. D. Structure-Tuned Lead Halide Perovskite Nanocrystals. *Adv. Mater.* **2016**, *28*, 566–573.

(36) Yin, B.; Cavin, J.; Wang, D.; Khan, D.; Shen, M.; Laing, C.; Mishra, R.; Sadtler, B. Fluorescence Microscopy of Single Lead Bromide Nanocrystals Reveals Sharp Transitions during Their Transformation to Methylammonium Lead Bromide. *J. Mater. Chem. C* **2019**, *7*, 3486–3495.

(37) Ahmad, S.; Kanaujia, P. K.; Niu, W.; Baumberg, J. J.; Vijaya Prakash, G. In Situ Intercalation Dynamics in Inorganic–Organic Layered Perovskite Thin Films. *ACS Appl. Mater. Interfaces* **2014**, *6*, 10238–10247.

(38) Dahl, J. C.; Osowiecki, W. T.; Cai, Y.; Swabeck, J. K.; Bekenstein, Y.; Asta, M.; Chan, E. M.; Alivisatos, A. P. Probing the Stability and Band Gaps of Cs 2 AgInCl 6 and Cs 2 AgSbCl 6 Lead-Free Double Perovskite Nanocrystals. *Chem. Mater.* **2019**, *31*, 3134–3143.

(39) Lu, C.; Wright, M. W.; Ma, X.; Li, H.; Itanze, D. S.; Carter, J. A.; Hewitt, C. A.; Donati, G. L.; Carroll, D. L.; Lundin, P. M.; et al. Cesium Oleate Precursor Preparation for Lead Halide Perovskite Nanocrystal Synthesis: The Influence of Excess Oleic Acid on Achieving Solubility, Conversion, and Reproducibility. *Chem. Mater.* **2019**, *31*, 62–67.

(40) Imran, M.; Caligiuri, V.; Wang, M.; Goldoni, L.; Prato, M.; Krahne, R.; De Trizio, L.; Manna, L. Benzoyl Halides as Alternative Precursors for the Colloidal Synthesis of Lead-Based Halide Perovskite Nanocrystals. *J. Am. Chem. Soc.* **2018**, *140*, 2656–2664.

(41) McKinney, W. Data Structures for Statistical Computing in Python. In *Proceedings of the 9th Python in Science Conference*; van der Walt, S., Millman, J., Eds.; 2010; pp 51–56.

(42) Savitzky, A.; Golay, M. J. E. Smoothing and Differentiation of Data by Simplified Least Squares Procedures. *Anal. Chem.* **1964**, *36*, 1627–1639.

(43) Virtanen, P.; Gommers, R.; Oliphant, T. E.; Haberland, M.; Reddy, T.; Cournapeau, D.; Burovski, E.; Peterson, P.; Weckesser, W.; Bright, J.; et al. SciPy 1.0: Fundamental Algorithms for Scientific Computing in Python. *Nat. Methods* **2020**, *17*, 261–272.

(44) Pedregosa, F.; Weiss, R.; Brucher, M.; Pedregosa, F. et al.; Pedregosa, F.; Varoquaux, G.; Gramfort, A.; Michel, V.; Thirion, B.; Grisel, O.; et al. Scikit-Learn: Machine Learning in Python. *J. Mach. Learn. Res.* **2011**, *12*, 2825–2830.

(45) Dursun, I.; De Bastiani, M.; Turedi, B.; Alamer, B.; Shkurenko, A.; Yin, J.; El-Zohry, A. M.;

Gereige, I.; AlSaggaf, A.; Mohammed, O. F.; et al. CsPb 2 Br 5 Single Crystals: Synthesis and Characterization. *ChemSusChem* **2017**, *10*, 3746–3749.

(46) Qin, Z.; Dai, S.; Hadjiev, V. G.; Wang, C.; Xie, L.; Ni, Y.; Wu, C.; Yang, G.; Chen, S.; Deng, L.; et al. Revealing the Origin of Luminescence Center in 0D Cs 4 PbBr 6 Perovskite. *Chem. Mater.* **2019**, *31*, 9098–9104.

(47) Eijkelenkamp, A. J. H.; Vos, K. Reflectance Measurements on Single Crystals of PbFCl, PbFBr, and PbBr2. *Phys. status solidi* **1976**, *76*, 769–778.

(48) Yoon, S. J.; Stamplecoskie, K. G.; Kamat, P. V. How Lead Halide Complex Chemistry Dictates the Composition of Mixed Halide Perovskites. *J. Phys. Chem. Lett.* **2016**, *7*, 1368–1373.

(49) Kim, S.-J.; Koh, K.; Lustig, M.; Boyd, S.; Gorinevsky, D. An Interior-Point Method for Large-Scale -Regularized Least Squares. *IEEE J. Sel. Top. Signal Process.* **2007**, *1*, 606–617.

(50) Friedman, J.; Hastie, T.; Tibshirani, R. Regularization Paths for Generalized Linear Models via Coordinate Descent. *J. Stat. Softw.* **2010**, *33*, 1–22.

(51) Riedinger, A.; Ott, F. D.; Mule, A.; Mazzoti, S.; Knüsel, P. N.; Kress, S. J. P.; Prins, F.; Erwin, S. C.; Norris, D. J. An Intrinsic Growth Instability in Isotropic Materials Leads to Quasi-Two-Dimensional Nanoplatelets. *Nat. Mater.* **2017**, *16*, 743–748.

(52) Ott, F. D.; Riedinger, A.; Ochsenbein, D. R.; Knüsel, P. N.; Erwin, S. C.; Mazzotti, M.; Norris, D. J. Ripening of Semiconductor Nanoplatelets. *Nano Lett.* **2017**, *17*, 6870–6877.

(53) Knüsel, P. N.; Riedinger, A.; Rossinelli, A. A.; Ott, F. D.; Mule, A. S.; Norris, D. J. Experimental Evidence for Two-Dimensional Ostwald Ripening in Semiconductor Nanoplatelets. *Chem. Mater.* **2020**, *32*, 3312–3319.

(54) Hui, J.; Jiang, Y.; Gökçinar, Ö. Ö.; Tang, J.; Yu, Q.; Zhang, M.; Yu, K. Unveiling the Two-Step Formation Pathway of Cs 4 PbBr 6 Nanocrystals. *Chem. Mater.* **2020**, acs.chemmater.0c00661.

(55) Feinberg, M. Chemical Reaction Network Structure and the Stability of Complex Isothermal Reactors—I. The Deficiency Zero and Deficiency One Theorems. *Chem. Eng. Sci.* **1987**, *42*, 2229–2268.

For table of contents only:

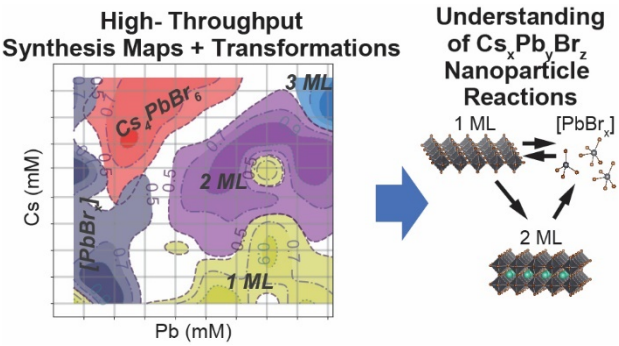
High- Throughput
Synthesis Maps + Transformations
Cs4PbBr6
3 ML
2 ML
1 ML
[PbBrx]
Cs (mM)
Pb (mM)
Understanding
of CsxPbyBrz
Nanoparticle
Reactions
1 ML
[PbBrx]
2 ML